Research Square

Preprints are preliminary reports that have not undergone peer review.
They should not be considered conclusive, used to inform clinical practice,
or referenced by the media as validated information.

Molecular level mechanism of carbon capture in linde type zeolite and how carbon templating enhances its thermal stability of CO2 adsorption

Collins Wafula
Jaramogi Oginga Odinga University of Science and Technology
Fredrick Okumu
Jaramogi Oginga Odinga University of Science and Technology
Gershom Mutua
Masinde Muliro University of Science and Technology
Anthony Pembere
apembere@jooust.ac.ke

Jaramogi Oginga Odinga University of Science and Technology https://orcid.org/0000-0002-9819-9155

Research Article

Keywords: Zeolite-templated carbon (ZTC), LTA zeolite, CO_2 adsorption, Carbon capture, Chemical vapor deposition (CVD), Microporous materials, Adsorption isotherm modeling

Posted Date: March 31st, 2026

DOI: https://doi.org/10.21203/rs.3.rs-9266095/v1

License: This work is licensed under a Creative Commons Attribution 4.0 International License.
Read Full License

Additional Declarations: The authors declare no competing interests.

Molecular level mechanism of carbon capture in linde type zeolite and how carbon templating enhances its thermal stability of CO_2 adsorption

Collins Wafula[1], Fredrick Okumu[1], Gershom Mutua[3], Anthony Pembere [1,2*]

[1]Department of Physical Sciences, Jaramogi Oginga Odinga University of Science and Technology, P.O Box 210 Bondo 40601, Kenya
[2]Michigan Institute for Data and AI in Society, University of Michigan. Weiser Hall, 500 Church Street, Suite 600, Ann Arbor, MI 48109-1042
[3]Department of Pure and Applied Chemistry, Masinde Muliro University of Science and Technology, P.O Box 190 Kakamega 50100, Kenya
*Email: apembere@jooust.ac.ke/apembere@umich.edu; https://orcid.org/0000-0002-9819-9155

Abstract

The rapid increase in atmospheric CO_2 concentrations remains a central driver of global climate change, necessitating the development of advanced carbon capture materials capable of operating efficiently under realistic conditions, including low CO_2 concentrations and elevated temperatures. Conventional adsorbents often suffer from high regeneration energy, corrosion, and limited thermal stability, while nature-based approaches lack scalability and permanence. These challenges underscore the need for robust, high-performance materials for next-generation carbon capture technologies. In this work, we investigate the carbon capture capacity of Linde Type A (LTA) zeolite, and the effect of carbon templating on its thermal stability for CO_2 adsorption. Grand Canonical Monte Carlo (GCMC) simulations reveal that the LTA framework is more sensitive to CO_2 adsorption, showing larger energetic changes, increased internal stress, and reduced mechanical rigidity. In contrast, LTA derived zeolite templated carbon (ZTC) exhibits superior structural resilience, pore accommodation, with minimal energy perturbations, and sustained mechanical stability. Temperature-dependent simulations further show that, although CO_2 uptake decreases with increasing temperature in both materials, the LTA-derived ZTC retains significantly higher adsorption capacity at elevated temperatures, demonstrating enhanced thermal stability. Experimental CO_2 adsorption measurements corroborate the simulation results, revealing improved high-temperature performance of the templated carbon relative to the parent zeolite. Overall, this study demonstrates that carbon templating is an effective strategy for transforming crystalline zeolites into thermally robust carbon adsorbents.

Keywords: Zeolite-templated carbon (ZTC), LTA zeolite, CO_2 adsorption, Carbon capture, Chemical vapor deposition (CVD), Microporous materials, Adsorption isotherm modeling

1.0 Introduction

The increase in atmospheric carbon dioxide (CO_2) concentration, due to human activities such as industrialization, urbanization, deforestation, and agricultural production, is the one of the major causes of global warming [1]. The effects of climate change are becoming increasingly apparent, particularly through severe storms, forest fires, and floods [2]. Furthermore, the melting of polar ice caps and rising sea levels have intensified the frequency of flooding, submerging coastal areas and causing significant damage to infrastructure and populations [3]-[4]. It is therefore essential to reduce greenhouse gas emissions [5] and to urgently develop effective carbon capture and storage technologies [6]. Various methods of CO_2 capture have been investigated, including direct air capture (DAC), where a sorbent material directly captures CO_2 using physical filters containing liquid or solid sorbents that chemically bind or adsorb CO_2 molecules, allowing other air components to pass through. Once the carbon dioxide is captured, heat is used to release it from the solvent or sorbent to be stored. This process regenerates the solvent or sorbent for a new capture cycle. Direct carbon capture (DAC) has the advantage of requiring little practical scaling expertise, a relatively small footprint, and high flexibility [7]. However, it is an energy-intensive method: capturing one tonne of CO_2 with a fossil fuel-powered DAC would result in the emission of the equivalent of 3.5 tonnes of CO_2, making it less efficient [8]. Oxy-combustion is another carbon capture and storage (CCS) technique that involves burning a fossil fuel with pure oxygen rather than air. It is a very promising method, although it requires a very large amount of energy to produce high-purity oxygen. In addition, combustion in a pure oxygen medium generates high temperatures. Consequently, large quantities of combustion gases must be recycled to maintain reasonable temperatures, making it an expensive CCS method [9].

Zeolites, three-dimensional microporous crystalline aluminosilicates, have been the subject of studies that have demonstrated their potential as high-performance materials for CO_2 capture. This is due to their large specific surface area, their tunable porous structure, and their good chemical stability [10]. They fall into two main categories: natural zeolites, formed by the crystallization of ash and rock layers from volcanic eruptions under the influence of groundwater or alkaline/saline lakes, and synthetic/artificial zeolites, crystalline aluminosilicates obtained by a thermal process. More than 50 natural zeolites have been identified; the most common being analcime, chabazite, clinoptilolite, erionite, ferrierite, heulandite, laumontite, mordenite, and phillipsite. More than 150 zeolites have been synthesized, the most common being zeolites A, X, Y, and ZSM-5. Zeolites are widely used as catalysts in the petrochemical industry, particularly in fluidized bed catalytic cracking, where they confine molecules to small spaces, inducing changes in their structure and reactivity. The acidic forms of zeolites prepared in this way are often strong solid acids, facilitating many acid-catalyzed reactions, such as isomerization, alkylation, and catalytic cracking [11]. They have also demonstrated great potential for the adsorption of pharmaceutical pollutants [28], heavy metals adsorption [29-31] and anions removal from waste water [32].

The production of zeolites, especially those with specific structures and compositions optimized for CO_2 capture, can be expensive. This cost can limit their use, particularly in large-scale industrial applications [12]. These limitations have led to increased interest in advanced materials called zeolite templated carbons (ZTCs), which are ordered microporous carbons synthesized using zeolites as a sacrificial matrix [13]. Due to their unique high-temperature and high-pressure resistance properties, zeolites can serve as rigid matrices for the synthesis and preparation of carbon nanomaterials by chemical vapor deposition (CVD) [14]. The synthesis of

these carbons is achieved by deposition of carbon within the pores of the zeolite via the pyrolytic carbonization of organic compounds [15]. The use of zeolites as a rigid matrix has generated considerable interest in the preparation of well-ordered porous carbon materials with controlled pore size and particle morphology. Furthermore, the zeolite matrix can often be partially or fully recovered and reused in subsequent cycles, thus reducing material consumption and promoting a circular and renewable synthesis cycle. ZTCs are now a well-established class of microporous carbons exhibiting the textural and morphological properties of matrix zeolites [16]. Their synthesis relies primarily on two common techniques. The first technique is the template synthesis method where materials are created with specific shapes and a structure using a template that directs the formation of the target material. The second, chemical vapor deposition (CVD), is a vacuum deposition method used to produce high-quality, high-performance solid materials. It involves exposing a zeolite matrix to a carbonaceous gas, such as methane or acetylene, in a CVD reactor to facilitate carbon deposition within the zeolite pores. ZTCs are characterized by their chemical inertness, high thermal stability, and good mechanical stability. Their high specific surface area and large pore volume have generated increasing interest over the past decade for new applications, including catalysis, drug delivery, fuel cells, supercapacitors, batteries, and adsorption/separation [17]. Structured porous carbons have the advantage of being readily functionalized with various dopants, making them ideal for catalysis, energy storage and conversion, sensors, and environmental applications [18]. Post-synthetic surface functionalization enhances the properties of nanocarbons, such as selective adsorption, charge storage, and increasing the number of catalytic sites. For example, the potential of nitrogen-doped zeolite-structured carbons for efficient CO_2 capture has been demonstrated, highlighting the importance of nitrogen species composition for optimizing adsorption

performance [19]. Another study showed that a high content of basic nitrogen species in nitrogen-doped ZTCs is crucial for improved CO_2 capture [20]. ZTCs are promising materials for CO_2 capture due to their uniform microporosity, extensive microporosity, very large specific surface area (~4000 $m^2 g^{-1}$), good compatibility with chemical modifications, and remarkable flexibility/elasticity [21]. These materials are also used in various processes such as hydrogen and methane storage, liquid-phase adsorption, catalysis, supercapacitors, batteries, and fuel cells [13]. In this study, we investigate the molecular-level mechanisms of CO_2 adsorption in Linde Type A (LTA) zeolite and its corresponding zeolite-templated carbon (ZTC), and further examine how carbon structuring of Linde type A zeolite (LTA) improves the thermal stability of CO_2 adsorption. Grand canonical Monte Carlo (GCMC) simulations are used to study the temperature-dependent CO_2 adsorption behavior of the initial LTA zeolite and LTA-derived ZTCs over a wide temperature range. We then validate the simulation results by synthesizing the ZTC via chemical vapor deposition [22] and experimentally evaluating its carbon dioxide adsorption performance.

2.0 Materials and Methods

2.1 Molecular dynamics simulations

The crystal structure of LTA zeolite (Figure 1) was obtained from the International Zeolite Association (IZA) structure database [25]. The corresponding zeolite matrix carbon (ZTC) structure derived from LTA was adapted from the work of Erik Braun et al., generated by a zeolite templating approach [26]. All structures were imported into BIOVIA Materials Studio [27] and processed under three-dimensional periodic boundary conditions (PBCs) to simulate infinite crystal systems and eliminate surface effects. CO_2 was modeled as a rigid linear triatomic molecule. Lennard-Jones parameters and charges were obtained from standard force field

libraries (conforming to COMPASS parameterization). CO_2 adsorption was simulated using the grand canonical Monte Carlo (GCMC) ensemble, where the chemical potential (μ), system volume (V), and temperature (T) are fixed, while the number of adsorbed molecules (N) fluctuates. The thermodynamic behavior of the system is governed by the grand canonical partition function;

$$\Xi(\mu, V, T) = \sum_{N=0}^{n} \frac{e\beta\mu N}{N!\,\Lambda 3} \int exp[-\beta U(r^N)] dr N$$

Where $\beta = 1/k_B T$ is the universe thermal energy, K_B is the Boltzmann constant, Λ is the thermal de Broglie wavelength, $U(r^N)$ is the total potential energy of the system and r^N represents the configurational coordinates of N molecules. The ensemble-averaged number of adsorbed molecules is obtained as:

$$\langle N \rangle = \frac{1\delta ln\Xi}{\beta \delta u}$$

The configurational space was sampled using the Metropolis Monte Carlo algorithm, employing four fundamental trial moves: molecule insertion, molecule deletion, translation, rotation. The acceptance probability for a general trial move is given by:

$$P_{acc} = \min (1, \exp [-\beta (\Delta U - \mu \Delta N)]$$

For particle insertion and deletion, the acceptance probabilities explicitly account for phase space normalization, where insertion is given by:

$$P_{ins} = \min (1, \frac{V}{(N+1)\Lambda 3} \exp[-\beta(-\Delta U - \mu)]$$

On the other hand, deletion is given by;

$$P_{del} = \min (1, \frac{N\Lambda 3}{V} \exp [-\beta(\Delta U + \mu)]$$

These expressions ensure detailed balance and proper sampling of particle fluctuations in the grand canonical ensemble. The chemical potential of CO_2 is related to its fugacity through:

$$u = u\circ + kBTln\left(\frac{f}{f}\circ\right)$$

where f is the fugacity of CO_2, f^o is the reference fugacity (typically 1 atm) and u^o is the standard chemical potential. Fugacity values were used instead of pressure to account for non-ideal gas behavior at elevated pressures. Adsorption isotherms were computed over a range of fugacities under isothermal conditions at various temperatures. Each state point consisted of equilibration cycles ensuring system stabilization and production cycles used for ensemble averaging. The average adsorption loading was calculated as:

$$N = \frac{1}{M}\sum Ni$$

where M is the number of sampled configurations during the production phase. All intermolecular and framework–adsorbate interactions were described using the COMPASS force field. The total potential energy of the system is expressed as:

$$U_{\text{total}} = U_{\text{bonded}} + U_{\text{non-bonded}}$$

For rigid frameworks, bonded contributions are negligible, and the energy is dominated by non-bonded interactions:

$$U_{non\text{-}bonded} = U_{vdw} + U_{elec}$$

Van der Waals interactions modelled using the Lennard-Jones potential

$$ULJ(rij) = 4\varepsilon ij\left[\left(\frac{\sigma}{r}\right)^{12} - \left(\frac{\sigma}{r}\right)^{6}\right]$$

Where E_{ij} is the well depth, Σ_{ij} is the collision diameter, r_{ij} is the inter atomic distance.

The electrostatic interactions were computed using coulomb's law:

$U_{elec}(r_{ij}) = \frac{qiqj}{4\pi\varepsilon 0rij}$, where qi and qj are partial charges and ε_0 is the vacuum permittivity. The long range electrostatic interactions were treated using the Ewald summation method, ensuring accurate evaluation under periodic boundary conditions:

$$U_{Ewald} = U_{real} + U_{reciprocal} + U_{self}$$

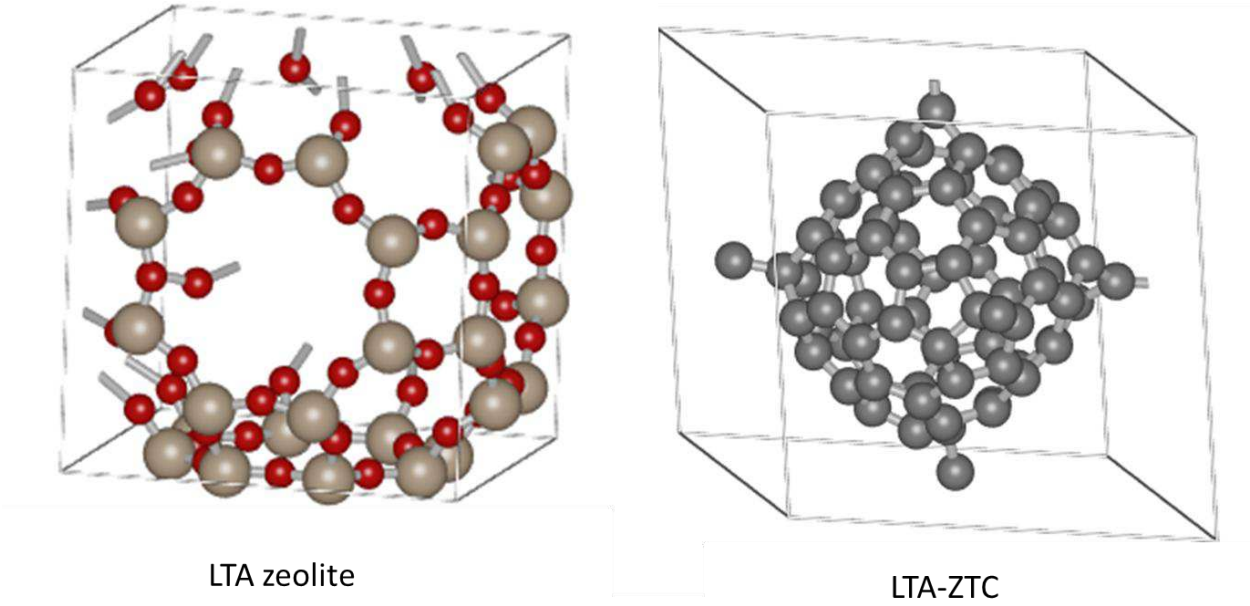


Figure 1. Structures for LTA zeolite and LTA ZTC

2.2 Experimental section

The synthesis of LTA-ZTC was carried out by chemical vapor deposition (CVD). Ten grams of LTA were impregnated with isooctane (a carbon precursor) and allowed to gel overnight. The resulting gel was then carbonated under an inert atmosphere at 600 °C for 4 hours and subsequently cooled to room temperature. The matrix was removed by dissolving the zeolitic

structure in 0.05 mol of hydrofluoric acid. The product was filtered, washed with demineralized water to remove all traces of acid, and then dried according to the protocol described by Khan et al. (2022) [24]. LTA-ZTCs were characterized by X-ray diffraction to identify the crystal structure and phase composition of the ZTC, by scanning electron microscopy to examine the morphology and surface topology of the zeolites and ZTCs, by transmission electron microscopy to study the internal structure and nanostructure of the zeolites and ZTCs, and by Fourier transform infrared (FTIR) spectroscopy to verify the presence of functional groups in the ZTCs.

The CO_2 used in this study was generated by the reaction between calcium carbonate and 1.0 M hydrochloric acid and used directly in the adsorption studies performed under ambient laboratory conditions. 10.0 g of calcium carbonate were placed in an Erlenmeyer flask. The mass of the empty adsorption column and the mass of the adsorption column containing the LTA zeolite were recorded. The Erlenmeyer flask was then connected to the adsorption column using transfer tubes. Hydrochloric acid was then added to the Erlenmeyer flask containing the calcium carbonate, allowing the released gas to pass through the adsorption column containing the zeolites. Hydrochloric acid was added gradually until the reaction stopped. The mass of the column containing the zeolite was then measured after adsorption to determine the mass of carbon dioxide adsorbed by the zeolite. The experiments were performed in triplicate to ensure reproducibility of the results. The mass of CO_2 adsorbed was determined gravimetrically.

3.0 Results and discussions

Grand canonical Monte Carlo (GCMC) simulations were used (Figure 2) to study CO_2 adsorption on an LTA-type zeolite at 375 K over a wide fugacity range (10–10,000 kPa). The resulting adsorption isotherm exhibits a characteristic type I (Langmuir type) profile, indicating microporous adsorption dominated by strong adsorbate-lattice interactions and a finite pore

volume. At low fugacity (10 kPa), CO_2 adsorption is minimal (0.177 molecules per unit cell), reflecting limited occupancy of high-energy adsorption sites. Similarly, the isosteric heat of adsorption ($Q_{st} \approx 6.2$ kcal/mol) suggests relatively weak initial interactions, likely governed by dispersive forces and quadrupole-lattice interactions typical of nonpolar structures. The absence of lattice charge in the model further reduces electrostatic contributions, explaining the low affinity in dilute media. When the fugacity reaches approximately 1000 kPa, a sharp increase in charge is observed (≈7.0 molecules/unit cell), marking the onset of micropore filling. This regime is associated with the preferential occupation of energetically favorable sites within the α cages of the LTA structure. The increase in Q_{st} to approximately 8.6 kcal/mol indicates a strengthening of adsorbate-structure interactions, as well as the emergence of cooperative adsorbate-adsorbate effects, where intermolecular interactions stabilize additional CO_2 molecules in the confined pore spaces. Above approximately 2000–4000 kPa, the isotherm begins to stabilize, with the charge approaching saturation (approximately 8.5–9.0 molecules/unit cell). This behavior reflects the progressive filling of the accessible pore volume and the decreasing availability of high-energy adsorption sites. In this intermediate to high pressure regime, the isosteric heat stabilizes around 9.0–9.3 kcal/mol, suggesting an equilibrium between adsorbate-lattice and adsorbate-adsorbate interactions. At the highest fugacities (8,000–10,000 kPa), the system reaches near-saturation with adsorption rates of approximately 10.5–10.6 molecules per unit cell. The slight increase in Q_{st} (up to approximately 10.6 kcal/mol) can be attributed to enhanced lateral interactions and stacking constraints within the confined microporous medium. The limited increase in the adsorption rate despite significant pressure increases confirms that adsorption is strongly limited by pore size, which is consistent with the fixed size of the LTA zeolite cavities. Monte Carlo analysis of acceptance rates reveals that insertion (creation)

probabilities decrease significantly with increasing fugacity (from ~10^{-2} to ~10^{-4}), reflecting the increasing difficulty of accommodating additional molecules in an increasingly crowded porous network. Conversely, the high acceptance rates for rotational and translational motions (>0.9 and ~0.4, respectively) indicate that configurational sampling remains effective even at high filling rates, thus ensuring reliable thermodynamic averages. The overall energy trend, with total system energy increasing from ~37 kcal/mol at low filling rates to ~2200 kcal/mol at saturation, is consistent with the cumulative contribution of intermolecular interactions. Importantly, the moderate value of Q_{st} for all fugacities (6–11 kcal/mol) suggests that CO_2 adsorption in neutral LTA is primarily of the physisorbent type, which is advantageous for regeneration but may limit selectivity under competitive adsorption conditions.

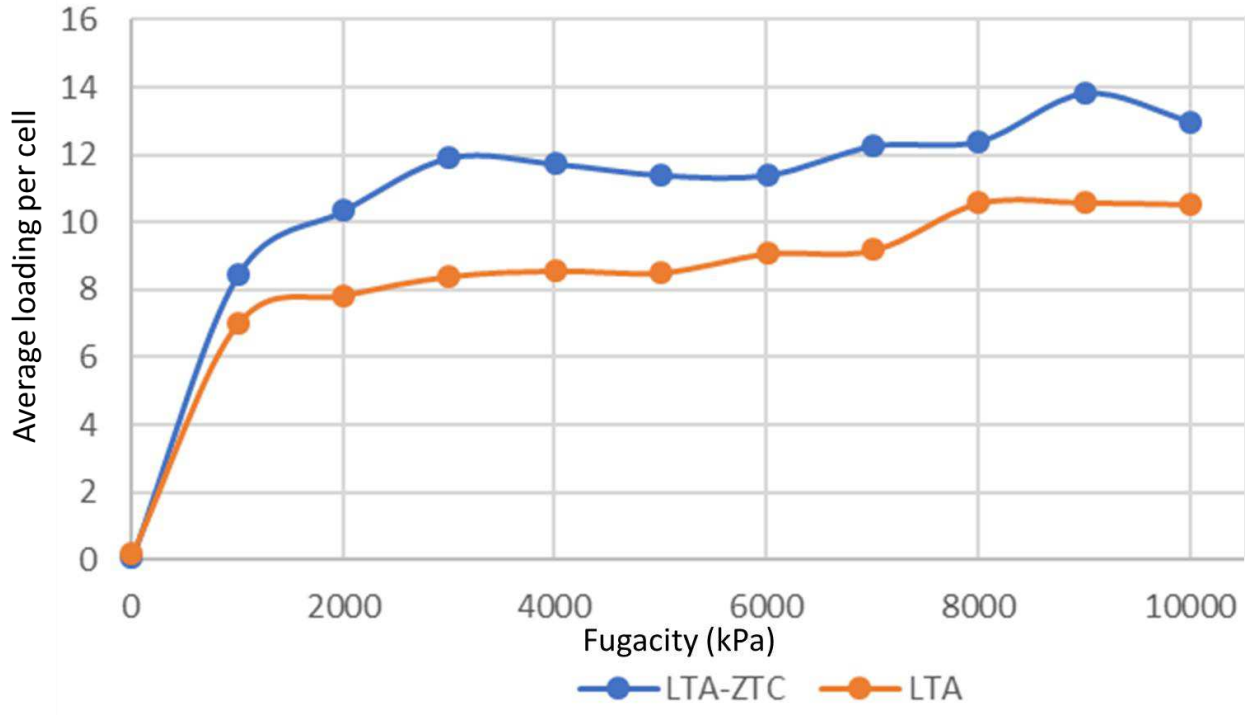


Figure 2. CO_2 Adsorption in LTA Zeolite and LTA-ZTC at 375 K

The adsorption behavior of CO_2 on LTA-structured carbon was also investigated using GCMC simulations at 375 K for a fugacity range of 10 to 10,000 kPa (Figure 2). Unlike the original LTA zeolite, the structured carbon exhibits a broader and more gradual adsorption isotherm, reflecting fundamental differences in surface chemistry and pore architecture. At low fugacity (10 kPa), CO_2 adsorption is extremely limited (0.044 molecules per cell), significantly lower than that observed for the zeolite. This is accompanied by a reduced isosteric heat of adsorption ($Q_{st} \approx 3.9$ kcal/mol), indicating weak initial adsorbate-surface interactions. This behavior is consistent with the largely nonpolar nature of carbon structures and the absence of strong electrostatic adsorption sites (e.g., polar cations or oxygen atoms within the structure), which are typically responsible for the increased affinity for CO_2 in zeolites. A sharp increase in adsorption is observed at moderate fugacity (~1000 kPa), where the charge reaches approximately 8.4 molecules per cell. This marks the onset of micropore filling, primarily due to van der Waals interactions and confinement effects. Compared to LTA zeolite, this transition is more abrupt, suggesting a more uniform energy landscape within the carbon pores, in contrast to the heterogeneous site distribution in crystalline zeolites. As the fugacity increases further (2000–4000 kPa), the system exhibits continuous adsorption, reaching approximately 11.7–11.9 molecules per cell. Notably, this value exceeds the saturation capacity observed in LTA zeolite (~10.5 molecules per cell), indicating that carbon structuring introduces additional accessible pore volume or improved pore connectivity. This improvement is likely due to partial structural relaxation or the formation of secondary micropores during carbonization, which increases the effective adsorption space. At high fugacity ($\geq$ 7000 kPa), adsorption reaches saturation, with maximum loads on the order of 13–14 molecules per cell. The higher saturation capacity

compared to zeolite confirms that the tempered carbon structures can accommodate higher CO_2 densities, likely due to less restrictive pore geometries and reduced steric hindrance. The isosteric heat of adsorption increases progressively with the load, from approximately 3.9 kcal/mol at low coverage to approximately 10.3–10.7 kcal/mol at high fugacity. This trend reflects the increasing importance of adsorbate-adsorbate interactions in confined environments, particularly CO_2-CO_2 quadrupole interactions and stacking effects within micropores. The convergence of Q_{st} values at high loading to those observed in LTA zeolite suggests that, under dense stacking conditions, intermolecular interactions predominate over structure-specific effects. Monte Carlo statistics corroborate these observations. Insertion (creation) acceptance rates decrease significantly with increasing fugacity (from ~10^{-2} to ~10^{-4}), which is consistent with the progressive filling of pores and the reduction of accessible free volume. However, the relatively high acceptance rates for translation (~0.35–0.47) and rotation (~0.90+) indicate efficient configurational sampling, even under high density conditions. In terms of energy, the system exhibits a substantial increase in total energy (from approximately 9 kcal/mol at low charge to approximately 2700–2900 kcal/mol at saturation), reflecting cumulative intermolecular interactions and a higher adsorbate density than in the zeolite system. This is consistent with the higher maximum charge observed in structured carbon.

We also calculated the temperature-dependent CO_2 adsorption behavior for the initial LTA zeolite and the LTA-derived zeolite templated carbon (LTA-ZTC) to better understand the role of the carbon templating in enhancing adsorption stability at high temperatures (Figure 3). As shown by the adsorption profile, both materials exhibit a decrease in the number of CO_2 molecules adsorbed per unit cell as the temperature increases from 350 K to 530 K. This behavior is characteristic of physisorption processes, as increasing temperature raises the kinetic

energy of gas molecules, weakening adsorbate-adsorbent interactions and promoting desorption. At low temperatures, the initial LTA zeolite exhibits a higher CO_2 adsorption capacity than LTA-ZTC. For example, at 298 K, LTA zeolite adsorbs approximately 27 CO_2 molecules per unit cell, while LTA-ZTC adsorbs approximately 15. This higher adsorption capacity can be attributed to the strong electrostatic interactions between the CO_2 molecules and the polar aluminosilicate network of the zeolite. The presence of aluminum in the network and associated charge-compensating cations creates high-energy adsorption sites that strongly attract quadrupolar CO_2 molecules. Consequently, LTA zeolite exhibits a higher adsorption capacity at relatively low temperatures, where adsorption interactions predominate over thermal effects. However, as the temperature increases, the adsorption capacity of the zeolite decreases more rapidly than that of the carbon template material. Between 350 K and 470 K, CO_2 adsorption by LTA zeolite drops sharply, from approximately 27 to about 5 molecules per unit cell. In contrast, the decrease in LTA-ZTC's adsorption capacity is more gradual, from about 15 molecules at 350 K to about 8–9 molecules at 470 K. Above approximately 375 K, LTA-ZTC outperforms the reference zeolite, retaining a greater number of adsorbed CO_2 molecules at higher temperatures. At 500 K and 530 K, for example, LTA-ZTC maintains adsorption levels of approximately 6 and 5 molecules per unit cell, respectively, while LTA zeolite retains only about 4 and 3.

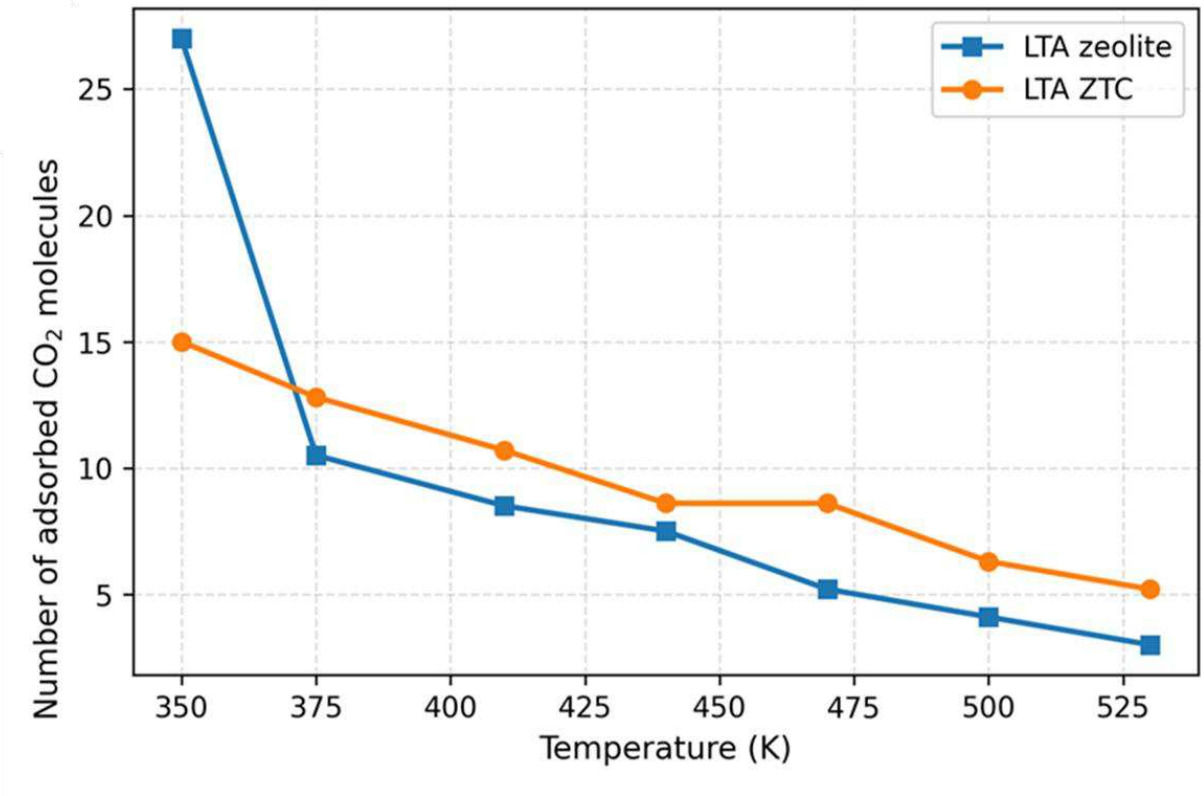


Figure 3. Calculated temperature-dependent CO_2 adsorption

Table 1. Structural properties of LTA and LTA-ZTC

Property	**Zeolite**	**ZTC**
Mass(g/mol)	1442.02320	912.81320
Density(kg/m^3)	1414.17084	886.03935
Helium void fraction	0.46581	0.90654
Specific volume(cm^3/g)	0.70713	1.12862
Accessible pore volume (cm^3/g)	0.32939	1.023
Volumetric surface area (m^2/cm^3)	1671.50232	2195.24217
Gravimetric surface area (m^2/g)	1181.9663	2477.58994

To better understand the adsorption mechanisms, we also calculated the structural properties of LTA zeolite and LTA-ZTC, as presented in Table 1. These properties highlight the significant transformation that occurs when the structure of Linde type A zeolite (LTA) is converted into zeolite templated carbon (LTA-ZTC) by the carbon tempering process. These modifications help to understand how tempering alters the pore architecture, density, and surface characteristics of

the material, thus influencing its CO_2 adsorption performance, particularly at high temperatures. The molar mass of the initial LTA zeolite (1442.02 g/mol) is significantly higher than that of the derived LTA-ZTC (912.81 g/mol). This reduction results from the removal of the inorganic aluminosilicate structure during the matrix removal step, which is typically performed by hydrofluoric acid etching. Once the silica and alumina components are removed, only the carbon replica of the porous structure remains, resulting in a lighter material. A similar trend is observed for density: LTA zeolite has a density of 1414 kg/m³, while LTA-ZTC has a lower density of 886 kg/m³. This reduction reflects the transition from a relatively dense aluminosilicate crystal lattice to a highly porous carbon structure. The lower density of LTA-ZTC is consistent with the formation of an open carbon lattice containing numerous micropores and voids inherited from the zeolitic matrix. The helium void fraction increases significantly, from 0.46581 in LTA zeolite to 0.90654 in LTA-ZTC, indicating that the carbon templated structure contains a much larger fraction of accessible void space. The helium void fraction is commonly used to estimate the total porosity of porous materials, as helium atoms can penetrate very small pores. The near-doubling of this fraction suggests that the carbon matrix process generates a highly porous network that closely replicates the topology of the original zeolite, while also introducing additional micro- and mesoporous features. This high porosity is beneficial to gas adsorption processes because it increases the number of available adsorption sites and facilitates molecular diffusion within the structure. The specific volume also increases, from 0.707 cm³/g in LTA to 1.1286 cm³/g in LTA-ZTC, thus confirming the development of a more open and extensive pore network in the structured carbon material. A higher specific volume indicates that each gram of material occupies a larger volume due to the increased internal void space. This structural expansion is consistent with the elimination of the inorganic network and the formation of a

carbon scaffold that retains the structured pore architecture but with less structural rigidity than the original zeolite. One of the most notable changes is observed in the accessible pore volume, which increases from 0.329 cm^3/g in LTA zeolite to 1.023 cm^3/g in LTA-ZTC. This represents a more than threefold increase in pore accessibility. The increase in accessible pore volume is particularly important for gas adsorption applications, as it directly determines the number of adsorption sites available for gas molecules such as CO_2. The large pore volume of LTA-ZTC suggests that the carbon replication process effectively preserves and expands the microporous network of the original zeolite while introducing additional porosity. The volumetric specific surface area increases from 1671.50 m^2/cm^3 for LTA zeolite to 2195.24 m^2/cm^3 for LTA-ZTC. This increase indicates that, even when normalized to volume, the carbon templated structure offers a larger internal surface area for adsorption interactions. A higher volumetric specific surface area enhances the material's adsorption potential because gas molecules interact with the internal pore surfaces. The increased specific surface area of LTA-ZTC suggests that the carbon templated network provides a more extensive adsorption interface than the original aluminosilicate structure. The most significant improvement is in the gravimetric specific surface area, which increases from 1181.97 m^2/g for LTA zeolite to 2477.59 m^2/g for LTA-ZTC. This substantial increase reflects the extremely high specific surface area characteristic of zeolite-templated carbons. All of these features improve the adsorption capacity and thermal stability of CO_2. The enlarged porous network allows CO_2 molecules to remain adsorbed even as the temperature increases, thus reducing the rate at which the capacity.

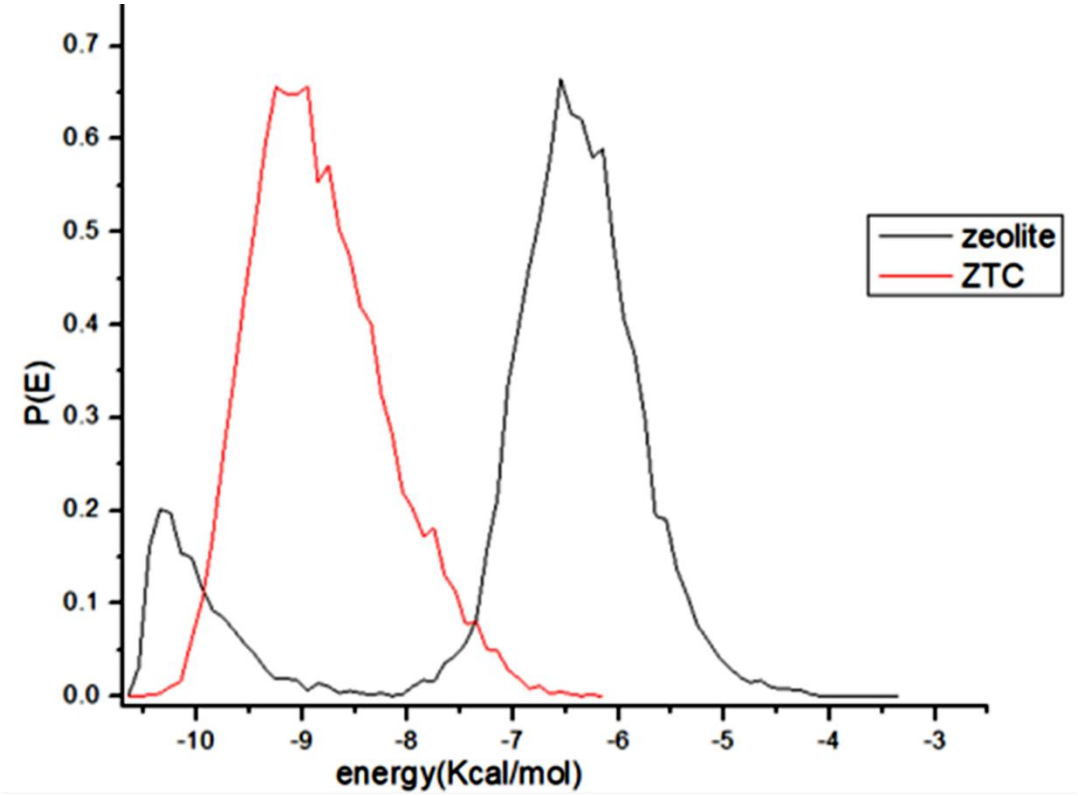


Figure 4. Energy distribution of CO_2 adsorption in LTA Zeolite and LTA-Derived ZTC at 375K

The energy distribution profiles (Figure 4) for CO_2 adsorption in LTA zeolite and LTA-derived zeolite-matrix carbon (LTA-ZTC) provide valuable information on the nature and intensity of adsorption interactions within these two materials. The probability distribution as a function of adsorption energy reflects the range and frequency of adsorption sites available for CO_2 molecules during the loading process. The distribution for LTA zeolite is centered on relatively high (less negative) adsorption energies, with a main peak around −6.5 kcal/mol. This indicates that CO_2 adsorption in the zeolite structure is dominated by moderately strong interactions. These interactions result primarily from electrostatic forces between the quadrupolar CO_2 molecules and the charged aluminosilicate structure, particularly the extralattice cations present in the LTA zeolite. These sites create localized, high-energy

adsorption centers where CO_2 molecules preferentially bind. The relatively narrow distribution suggests that adsorption occurs within well-defined microporous cages of the LTA crystal structure, where the adsorption environment is fairly uniform. In contrast, the energy distribution of LTA-ZTC is shifted toward lower (more negative) adsorption energies, with a peak centered around −9 kcal/mol. This shift indicates stronger overall adsorption interactions between the CO_2 molecules and the carbon structure. The broader distribution of adsorption energies observed for LTA-ZTC also suggests the presence of a more heterogeneous set of adsorption sites within the carbon structure. Unlike the highly ordered and chemically uniform adsorption sites of the zeolite structure, the structured carbon network contains a variety of microporous environments and surface defects that can contribute to stronger dispersive interactions with CO_2 molecules. The increased adsorption energy of LTA-ZTC can be attributed to several structural features introduced during the carbon structuring process. Structured carbon has a significantly larger specific surface area and accessible pore volume, resulting in a greater number of adsorption sites. Furthermore, the carbon structure provides extensive π-electron-rich surfaces, enhancing van der Waals interactions with CO_2 molecules. These dispersive interactions can generate higher adsorption energies, distributed throughout the microporous carbon network. Another important feature of the energy distribution of LTA-ZTC is its broader and more continuous range of adsorption energies compared to that of zeolite. This indicates that CO_2 molecules are exposed to multiple adsorption environments within the carbon structure, including narrow micropores, pore intersections, and surface defects generated during the structuring and etching processes. This heterogeneity is typical of zeolite-structured carbons and contributes to their excellent adsorption performance. These results confirm the improved adsorption behavior observed in temperature-dependent adsorption simulations. The higher and more widely

distributed adsorption energies in LTA-ZTC suggest that CO_2 molecules remain energetically stabilized within the carbon structure, even as thermal energy increases. Therefore, the structured carbon material is better able to retain CO_2 molecules at high temperatures than the original zeolite.

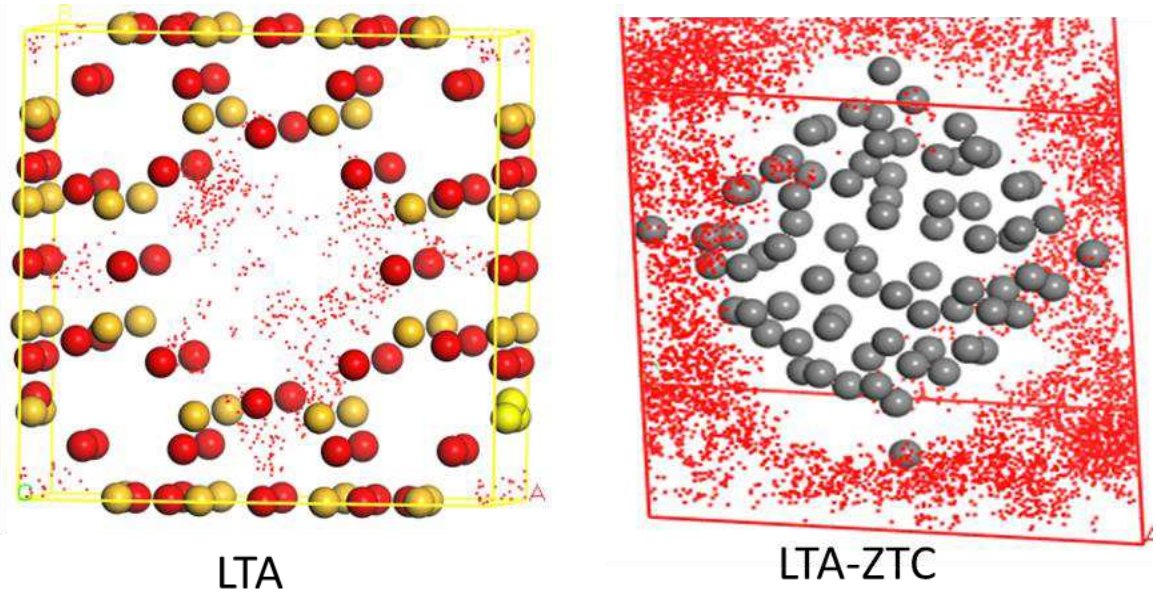


Figure 5. Spatial distribution of CO_2 molecules in LTA zeolite and LTA-derived ZTC at 375K

The spatial distribution of CO_2 molecules within LTA zeolite and LTA-ZTC provides important information on the influence of the internal porous architecture of both materials on their adsorption behavior (Figure 5). This figure illustrates representative configurations obtained through adsorption simulations, where the red dots represent CO_2 molecules and the lattice atoms correspond to the structural matrices of the adsorbents. In LTA zeolite, CO_2 molecules are primarily localized within the well-defined microporous cavities of the aluminosilicate crystal lattice. The distribution appears relatively localized and structured, reflecting the highly ordered pore system characteristic of LTA zeolites. The LTA lattice consists of interconnected α cages and smaller windows that impose geometric constraints on the movement and positioning of gas

molecules. Consequently, CO_2 molecules tend to accumulate near energetically favorable adsorption sites within these cages, often close to lattice oxygen atoms and extralattice cations. These strong, localized electrostatic interactions induce preferential adsorption at specific positions within the zeolite pores. However, the restricted pore opening and confined cage geometry limit the overall spatial distribution of CO_2 molecules, which can reduce adsorption flexibility at high temperatures. In contrast, LTA-derived ZTC exhibits a distinctly different adsorption profile. CO_2 molecules appear more widely distributed within the porous carbon structure, reflecting the more open and interconnected pore network produced during the carbon tempering process. Unlike the zeolite crystal lattice, the carbon replica consists of a continuous microporous carbon matrix that preserves the overall topology of the original zeolite but introduces additional pore connectivity and surface heterogeneity. Consequently, CO_2 molecules can occupy a wider variety of adsorption sites throughout the material. The more uniform and extensive distribution of CO_2 within the LTA-ZTC structure is consistent with its larger accessible pore volume, higher specific surface area, and greater porosity compared to the original zeolite. These structural features provide a greater number of adsorption sites and facilitate improved molecular diffusion within the carbon lattice. The presence of extensive carbon surfaces also promotes dispersive interactions between CO_2 molecules and pore walls, thus enabling adsorption across the entire microporous lattice rather than being confined to discrete, high-energy sites. This difference in adsorption distribution helps explain the improved adsorption stability of LTA-ZTC observed in temperature-dependent simulations. While adsorption in the zeolite network is dominated by specific high-energy sites whose efficiency decreases with increasing temperature, the carbon matrix structure offers a broader distribution

of adsorption environments. This allows CO_2 molecules to remain adsorbed within the porous network even when thermal agitation increases.

Table 2. Dynamics average values

System	Total Energy	Temperature (K)	Pressure (GPa)	Volume Stability
Unloaded LTA	551.162	304.23	-4.633	Constant
Loaded LTA	178.524	222.24	5.925	Constant
Unloaded LTA-ZTC	263.458	152.65	6.945	Constant
Loaded LTA-ZTC	285.771	165.48	7.012	Constant

Table 3. Anneal simulation average values

System	Total Energy	Temperature (K)	Pressure (GPa)	Volume
Unloaded LTA	870.639	397.16	-4.657	Constant
Loaded LTA	258.888	399.57	6.805	Constant
Unloaded LTA-ZTC	351.956	398.08	7.675	Constant
Loaded LTA-ZTC	374.882	401.12	7.732	Constant

The molecular dynamics simulations (Table 2) further demonstrate differences in dynamic behavior. Unloaded LTA operates near room temperature with slightly negative pressure, implying a mild tensile state within the framework. When loaded with CO_2, pressure shifts to strongly positive values, indicating adsorption-induced compressive stress in the cages. Conversely, LTA-ZTC systems maintain consistently positive pressures even before loading, reflecting a naturally compressive internal environment. CO_2 loading produces only minor changes in energy, temperature, and pressure for LTA-ZTC, indicating better dynamic stability compared to the zeolite framework. Similar trends are in the quench and anneal simulations (Table 3), where all systems remain structurally stable with constant volumes. In LTA, CO_2

loading significantly alters energy and pressure conditions, shifting the framework from tensile to compressive behavior. LTA-ZTC shows smaller variations in these parameters, further supporting the idea that the carbon template provides improved structural resilience during thermal and dynamic relaxation processes. Under shear simulations (Table 4), the frameworks maintain structural integrity under applied stress. Loaded LTA exhibits lower viscosity and moderate shear response, indicating increased flexibility. In contrast, LTA-ZTC systems display higher viscosity and stronger compressive responses, suggesting greater resistance to shear deformation due to the reinforcing carbon network.

Table 4. Shear simulation average values

System	Total Energy	Shear Stress Behavior	Viscosity (cP)	Structural Integrity
Loaded LTA	204.048	Compressive minor shear	3.654	Maintained
Loaded LTA-ZTC	308.115	Higher compressive response	6.012	Maintained

Table 5. Summary of simulated mechanical properties (Hill averages)

System	Bulk Modulus (GPa)	Shear Modulus (GPa)	Young's Modulus (GPa)	Behavior
Unloaded LTA	54.60	40.69	~89	Rigid, isotropic-like
Loaded LTA	31.61	8.14	~23–26	Shear-flexible
Unloaded LTA-ZTC	48.12	35.22	~82	Rigid porous carbon
Loaded LTA-ZTC	44.75	28.64	~70	Moderately flexible

Finally, the mechanical property analysis (Table 5) confirms that both unloaded LTA and LTA-ZTC are relatively rigid, with high bulk and shear moduli. However, CO_2 loading significantly reduces the stiffness of LTA, particularly its shear modulus, indicating increased framework flexibility. LTA-ZTC retains relatively high bulk and shear moduli even after loading,

demonstrating that the carbon-templated structure maintains mechanical strength while still allowing moderate flexibility. Overall, the comparative simulations indicate that LTA frameworks are more sensitive to CO_2 adsorption, showing larger energetic changes, increased internal stress, and reduced mechanical rigidity. In contrast, LTA-ZTC exhibits superior structural resilience, pore accommodation, with minimal energy perturbations, and sustained mechanical stability.

The RDF profile (Figure 6) of the unloaded LTA zeolite exhibits sharp peaks at short radial distances, typically around ~1.6 Å, ~2.6–3.0 Å, and ~4.0–5.0 Å, corresponding to Si–O/Al–O bonds, O–O distances within tetrahedra, and longer-range framework correlations, respectively. These high intensity and narrow width peaks confirm the highly ordered crystalline nature of the LTA framework. The absence of additional peaks beyond the framework correlations indicates that the pores remain empty, with no guest-induced structural perturbation. These well-defined coordination shells provide specific adsorption sites that are crucial for subsequent CO_2 uptake.

Upon CO_2 loading, the RDF profile retains the characteristic framework peaks ~1.6 Å and ~2.6–3.0 Å, confirming structural stability, but shows enhanced intensity in the short-range region (~3.0–3.5 Å). This additional contribution is due to CO_2–framework interactions, particularly between CO_2 oxygen atoms and the framework cations or oxygen sites. The emergence or amplification of peaks in this region indicates strong localization of CO_2 within the pores. Furthermore, slight increases in peak intensity at longer distances (~4–6 Å) suggest structured arrangement of CO_2 molecules within the confined pore system. This shows that CO_2 adsorption in LTA is highly site-specific and dominated by strong electrostatic interactions.

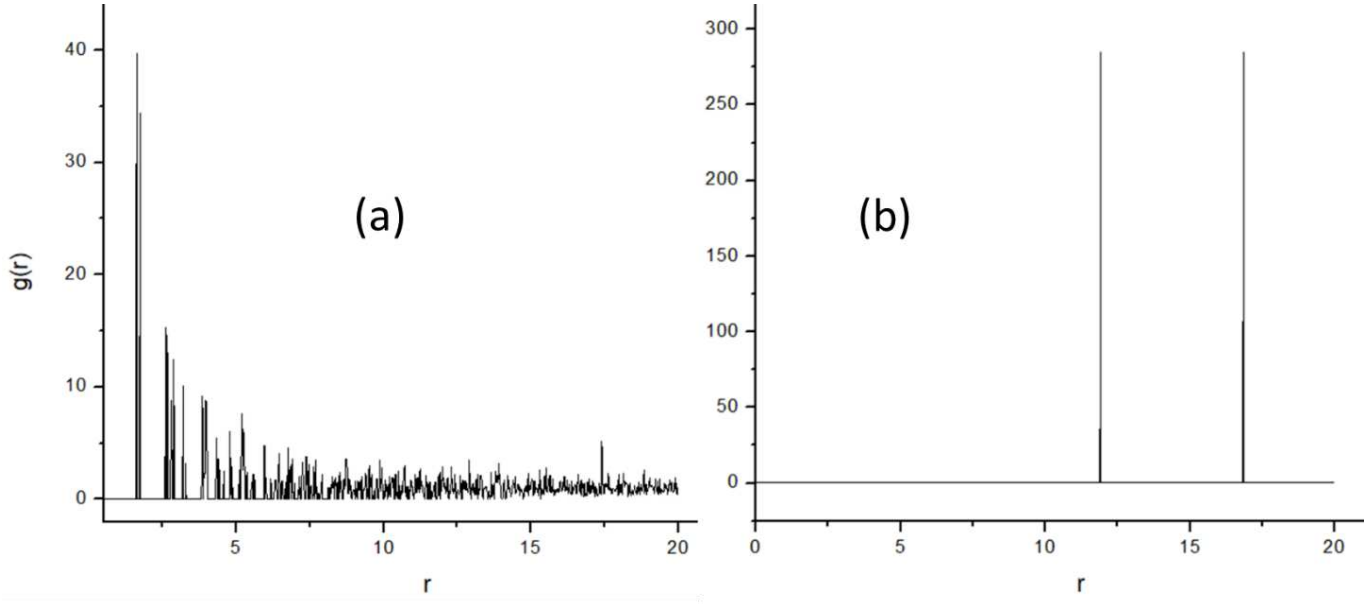


Figure 6: Radial distribution function (a) LTA zeolite before loading with CO_2
(b) LTA zeolite after being loaded with CO_2

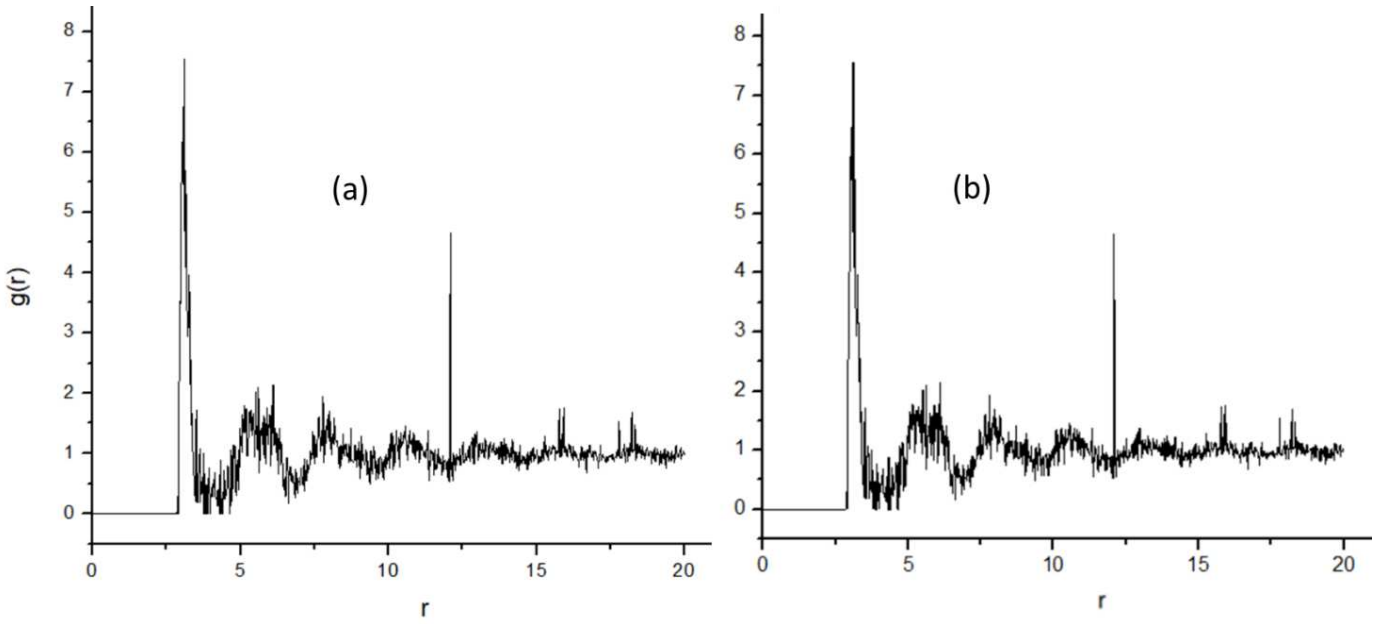


Figure 7: The radial distribution function (a) LTA ZTC before loading with CO_2 (b) LTA ZTC after loading with CO_2

The RDF profile of the unloaded LTA-ZTC displays broader peaks centered around ~1.4–1.5 Å, ~2.4–2.8 Å, and ~3.5–5.0 Å, corresponding to C–C bonding distances and short-range ordering within the carbon framework. Compared to LTA, these peaks are significantly broadened and reduced in intensity, indicating loss of long-range periodicity and increased structural disorder. The absence of sharp higher-order peaks reflects the amorphous nature of the carbon replica. Nevertheless, the presence of these peaks suggests retention of local structural features inherited from the zeolite template, forming a heterogeneous porous network. With CO_2 loading, the RDF profile of LTA-ZTC shows only modest changes, with slight increases in intensity around ~3.0–3.5 Å, corresponding to weak CO_2–carbon interactions. Unlike LTA zeolite, no sharp or well-defined new peaks emerge, indicating the absence of strong specific adsorption sites. The broad peaks in the ~4–6 Å region suggest a more diffuse distribution of CO_2 molecules within the pore network. This reflects adsorption dominated by van der Waals interactions rather than

electrostatics. The minimal shift in peak positions further indicates that CO_2 adsorption does not significantly alter the carbon framework, highlighting the weaker and less localized nature of adsorption in LTA-ZTC. From the above RDF peak, analysis confirms that CO_2 adsorption in LTA zeolite is characterized by strong, localized interactions at ~3.0–3.5 Å within a highly ordered framework, whereas LTA-ZTC exhibits weaker, broadly distributed interactions due to its disordered carbon structure.

To Validate the simulation results, LTA-derived ZTCs were synthesized by chemical vapor deposition (CVD) using isooctane as a carbon precursor, followed by the removal of the zeolite matrix by hydrofluoric acid etching. The resulting materials were characterized structurally and morphologically by X-ray diffraction (XRD), transmission electron microscopy (TEM), scanning electron microscopy (SEM), and Fourier transform infrared spectroscopy (FTIR). FTIR analysis (Figure 8 and 9) confirmed the successful transformation of the LTA zeolite into zeolite-matrixed carbon. This is evidenced by the spectrum of the LTA zeolite, dominated by O–H and Si–O–Al vibrations, indicating a well-crystallized, hydrated aluminosilicate structure. After synthesis, ZTC LTA exhibited characteristic C=C and C–O aromatic bands, confirming the formation of an sp^2 hybridized carbon network with oxygenated surface functional groups, favorable to CO_2 adsorption applications.

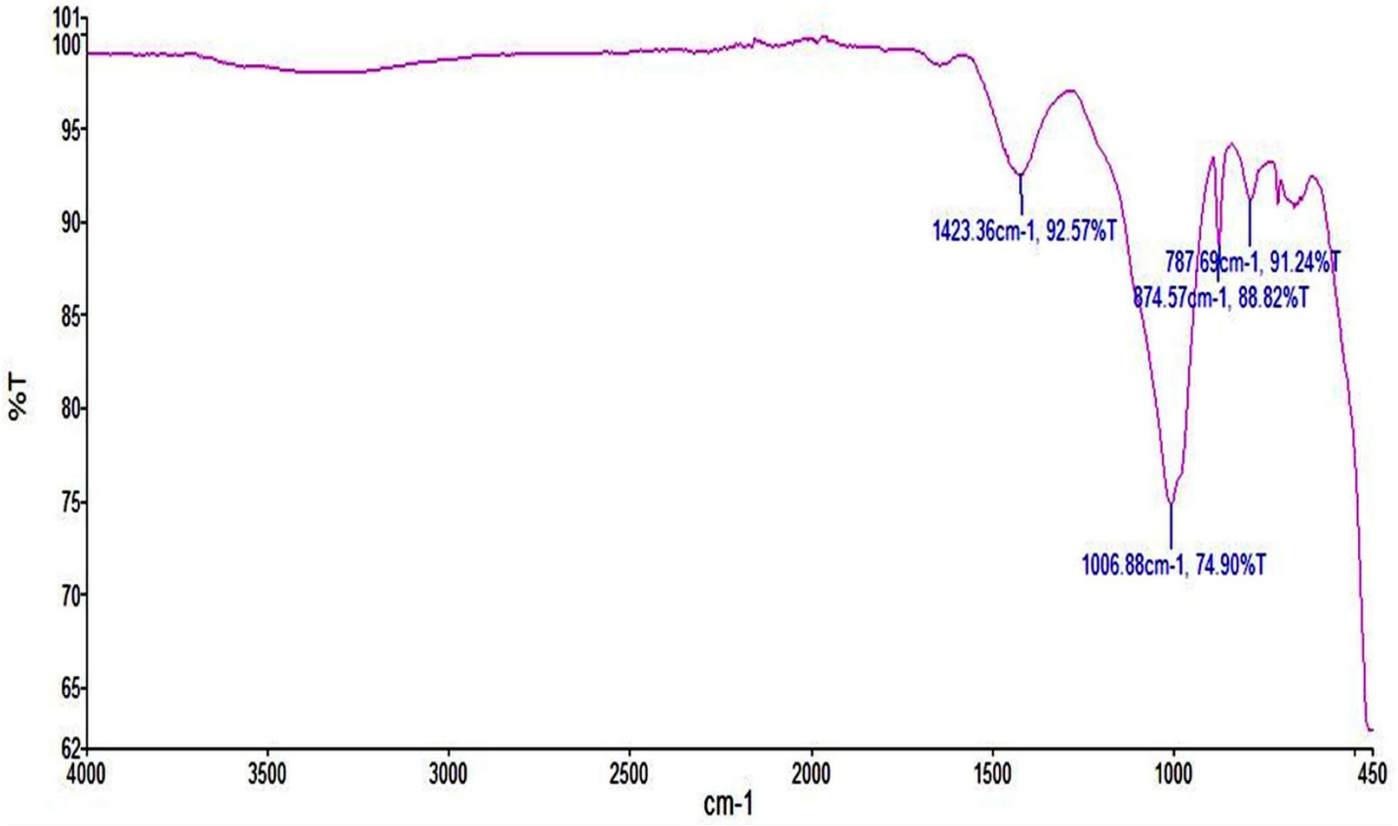


Figure 8. FTIR spectrum of LTA zeolite

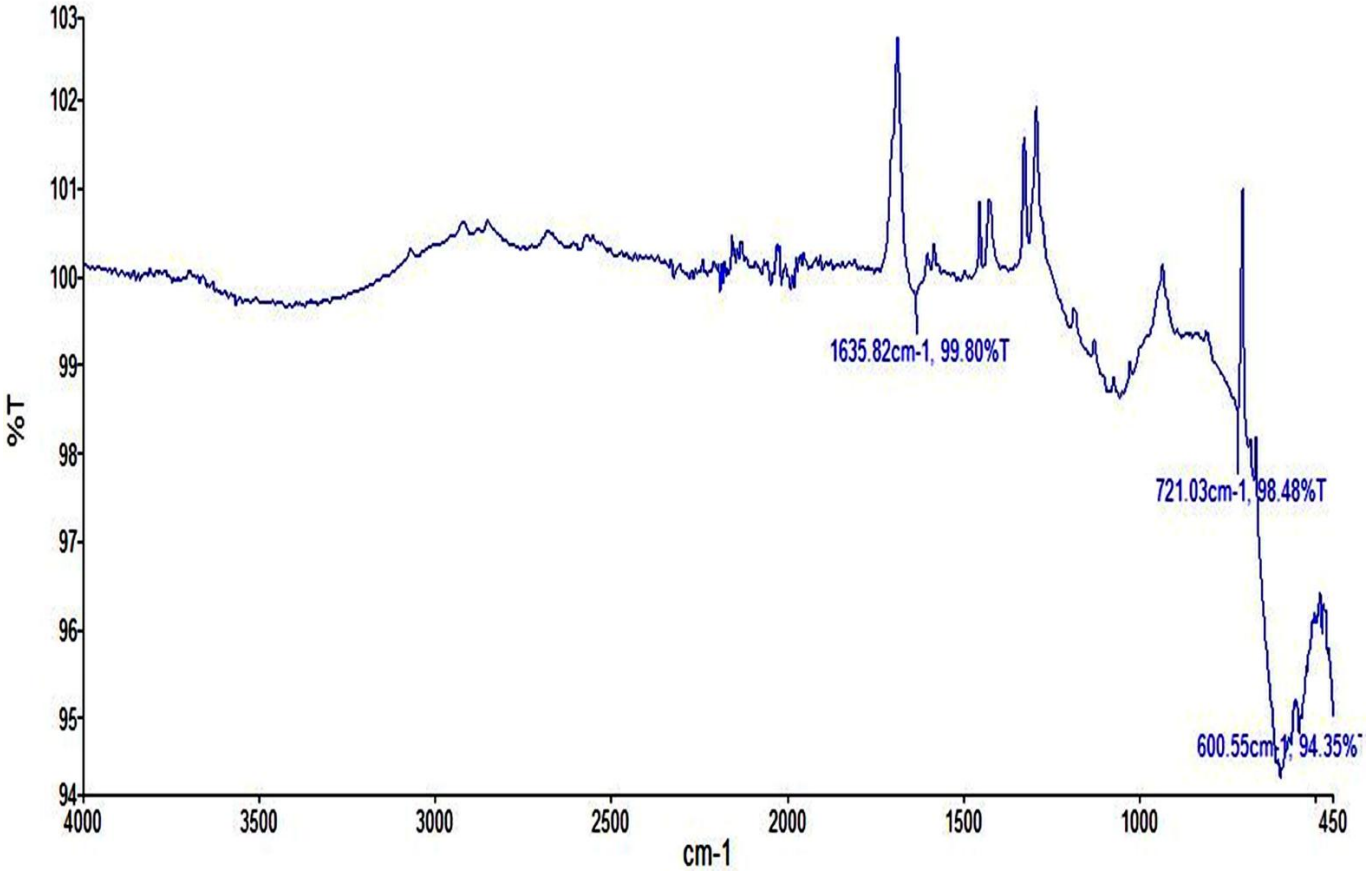


Figure 9: FTIR spectrum for LTA zeolite and LTA ZTC

The FTIR spectra (Figures 9 and 10) show the vibrational characteristics of LTA zeolite and LTA-ZTC. The LTA zeolite spectrum is characterized by strong Si–O–Si/Al–O–Si lattice vibrations. The dominant band at approximately 1000 cm^{-1} and the additional bands at approximately 660–750 and 450 cm^{-1} indicate the aluminosilicate crystal structure. In contrast, these characteristic lattice bands are absent in the LTA-ZTC spectrum, reflecting the removal of the zeolite matrix. LTA-ZTC then exhibits a distinct band at approximately 1550–1650 cm^{-1}, attributed to the stretching of C=C sp^2 bonds, as well as weaker C–O bands (approximately 1200–1400 cm^{-1}), characteristic of a carbon lattice. These spectral differences confirm that the

vibrations of its T–O–T structure define LTA, while LTA-ZTC is distinguished by the appearance of carbon-linked bands and the disappearance of zeolitic characteristics.

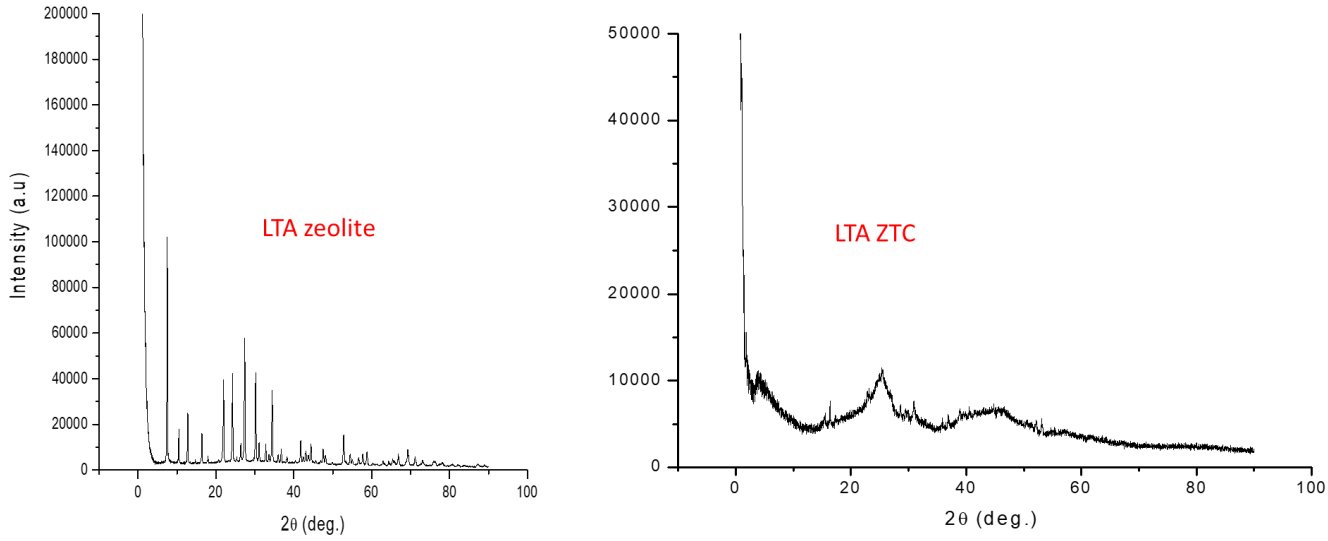


Figure 11: XRD pattern for LTA ZTC and LTA zeolite.

Table 6. Experimental results for percentage mass of adsorbed CO_2

Temperature (K)	% Mass of CO_2 adsorbed (LTA zeolite)	% Mass of CO_2 adsorbed (LTA ZTC)
298	5.09	2.872
350	4.978	2.234
450	2.106	4.096

The XRD pattern (Figure 11) of the LTA zeolite shows sharp reflections at 2θ ≈ 7.2°, 10.2°, 12.4°, and 16.1°, with additional peaks at ≈21.6°, 24.0°, 27.1°, and 29.9°, confirming a highly crystalline cubic aluminosilicate framework. In contrast, the LTA-ZTC pattern lacks all LTA reflections and is dominated by a broad peak at 2θ ≈ 23–26°, assigned to the (002) reflection of amorphous carbon, with a weak feature around ≈42–45° corresponding to disordered carbon. The

broad peaks indicate a highly amorphous, microporous carbon framework. Carbon dioxide adsorption performance was evaluated experimentally as seen in table 6. The experimental results corroborate the simulation predictions, confirming that carbon templating of the LTA framework leads to improved CO_2 adsorption stability at elevated temperatures.

Acknowledgement

A.P gratefully acknowledges funding support from Schmidt Sciences, and the Michigan Institute for Data and AI in Society at the University of Michigan and Kenya Education Network (KENET)

Declaration of conflict of interest

There are no conflicts of interest to declare.

References

1. Kabir, M., et al. Impacts of anthropogenic activities & climate change resulting from increasing concentration of Carbon dioxide on environment in 21st Century; A Critical Review. in IOP Conference Series: Earth and Environmental Science. 2023. IOP Publishing.
2. Meyer, A., et al., Extreme climate and weather events in a warmer world. 2023. 44.
3. Dube, K., G. Nhamo, and D.J.G. Chikodzi, Flooding trends and their impacts on coastal communities of Western Cape Province, South Africa. 2022. 87(Suppl 4): p. 453-468.
4. Cianconi, P., S. Betrò, and L. Janiri, The impact of climate change on mental health: a systematic descriptive review. Frontiers in psychiatry, 2020. 11: p. 490206.
5. Atedhor, G.O., Greenhouse gases emissions and their reduction strategies: Perspectives of Africa's largest economy. Scientific African, 2023. 20: p. e01705.
6. Dziejarski, B., R. Krzyżyńska, and K.J.F. Andersson, Current status of carbon capture, utilization, and storage technologies in the global economy: A survey of technical assessment. 2023. 342: p. 127776.
7. Cortinovis, S.R., Governing Carbon Removal: Deploying Direct Air Capture Amidst Canada's Energy Transition. 2023, University of Waterloo.

8. Foxall, R., Prospects For Direct Air Capture Onboard Floating Offshore Wind Turbines. 2023.

9. Yadav, S. and S.J.F. Mondal, A review on the progress and prospects of oxy-fuel carbon capture and sequestration (CCS) technology. 2022. 308: p. 122057.

10. Chen, L.-H., et al., Hierarchically structured zeolites: from design to application. 2020. 120(20): p. 11194-11294.

11. Gong, X., et al., First-generation organic reaction intermediates in zeolite chemistry and catalysis. 2022. 122(18): p. 14275-14345.

12. Boer, D.G., J. Langerak, and P.P. Pescarmona, Zeolites as selective adsorbents for CO2 separation. ACS Applied Energy Materials, 2023. 6(5): p. 2634-2656.

13. Choi, W., et al., Doping effect of zeolite-templated carbon on electrical conductance and supercapacitance properties. Carbon, 2022. 193: p. 42-50.

14. Miao, J., et al., Revival of zeolite-templated nanocarbon materials: recent advances in energy storage and conversion. Advanced Science, 2020. 7(20): p. 2001335.

15. Park, H., et al., Synthesis of zeolite-templated carbons using oxygen-containing organic solvents. Microporous and Mesoporous Materials, 2021. 318: p. 111038.

16. Blankenship, L.S. and R. Mokaya, Modulating the porosity of carbons for improved adsorption of hydrogen, carbon dioxide, and methane: a review. Materials Advances, 2022. 3(4): p. 1905-1930.

17. Benzigar, M.R., et al., Recent advances in functionalized micro and mesoporous carbon materials: synthesis and applications. Chemical Society Reviews, 2018. 47(8): p. 2680-2721.

18. Tian, W., et al., Porous carbons: structure-oriented design and versatile applications. Advanced Functional Materials, 2020. 30(17): p. 1909265.

19. Abdulkadir, B., et al., A concise review on surface and structural modification of porous zeolite scaffold for enhanced hydrogen storage. Chinese Journal of Chemical Engineering, 2024.

20. Lee, S.-K., et al., Base-type nitrogen doping in zeolite-templated carbon for enhancement of carbon dioxide sorption. 2022. 62: p. 102084.

21. Netto, M.S., et al., A novel zeolite template carbon (ZTC) for pharmaceutical removal in advanced wastewater treatment. 2024. 378: p. 113230.

22. Dziejarski, B., et al., CO2 capture materials: a review of current trends and future challenges. Materials Today Sustainability, 2023: p. 100483.

23. Kim, S., et al., PubChem 2019 update: improved access to chemical data. Nucleic acids research, 2019. 47(D1): p. D1102-D1109.

24. Khan, R., et al., Extraction processes for deriving cellulose: A comprehensive review on green approaches. 2022. 33(7): p. 2069-2090.

25. Baerlocher, Ch, Lynne B. McCusker, and David H. Olson. Atlas of zeolite framework types. Elsevier, 2007.

26. Braun, E., Lee, Y., Moosavi, S. M., Barthel, S., Mercado, R., Baburin, I. A., Proserpio, D. M., & Smit, B. (2018)

27. BIOVIA, Dassault Systèmes. "Materials Studio; Dassault Systèmes." *San Diego* (2017).

28. Wanyonyi, F. S.; Pembere, A.; Mutua, G. K.; Orata, F.; Louis, H., Computational Screening of Zeolites for the Adsorption of Selected Pharmaceutical Pollutants. *SN Applied Sciences* **2020**, *2*, 1901.

29. Wanyonyi, F. S.; Fidelis, T. T.; Mutua, G. K.; Orata, F.; Pembere, A. M., Role of Pore Chemistry and Topology in the Heavy Metal Sorption by Zeolites: From Molecular Simulation to Machine Learning. *Computational Materials Science* **2021**, *195*, 110519.

30. Wanyonyi, F. S.; Fidelis, T. T.; Louis, H.; Mutua, G. K.; Orata, F.; Rhyman, L.; Ramasami, P.; Pembere, A. M., Simulation Guided Prediction of Zeolites for the Sorption of Selected Anions from Water: Machine Learning Predictors for Enhanced Loading. *Journal of Molecular Liquids* **2022**, *355*, 118913.

31. Wanyonyi, F. S.; Orata, F.; Ramasami, P.; Ngeno, E.; Shikuku, V.; Gembo, R. O.; Mutua, G. K.; Pembere, A., Unlocking the Adsorptive Effectiveness of Naturally Occurring Heulandite Zeolite for the Removal of Po43− and No3− Anions from Wastewater. *Environmental Monitoring and Assessment* **2024**, *197*, 78.

32. Okello, F. O.; Fidelis, T. T.; Agumba, J.; Manda, T.; Ochilo, L.; Mahmood, A.; Pembere, A. J. M. T. C., Towards Estimation and Mechanism of Co2 Adsorption on Zeolite Adsorbents Using Molecular Simulations and Machine Learning. **2023**, *36*, 106594.